A FUNDAMENTAL STUDY OF GIBBSITE SCALE NUCLEATION ON MILD STEEL

Loan M, Klauber C* and Vernon C

CSIRO Light Metals Flagship / Parker CRC for Integrated Hydrometallurgy Solutions
CSIRO Minerals, Waterford, WA, Australia

Abstract

A fundamental understanding of the initial stages of scale formation and the factors that affect it is critical to the development of long-term strategies for scale inhibition. The nature of gibbsite scale nucleation on 1020 mild steel surfaces has been investigated using a temperature controlled laminar flow-through cell and X-ray photoelectron spectroscopy (XPS). The Fe 2p and Fe 3p behaviour was analysed by linear least squares component analysis to avoid the problems normally associated with iron peak fitting. This indicated that mild steel oxidized to a dry-air or Bayer liquor stable thin magnetite layer. A preliminary model has been quantitatively determined that describes the gibbsite precipitation on the mild steel as initially 1-2 monolayers of gibbsite (~0.2 to 0.4 nm) but up to 6 layers rapidly forming on a stable magnetite layer ~5 nm thick. After an induction period larger 3-dimensional gibbsite crystals nucleated and displayed pronounced two-stage static charging. Significantly, this work demonstrated that the initial liquor interaction is a precipitation reaction onto the mild steel magnetite and not a solids settling phenomenon.

Notation and units

X-ray photoelectron spectroscopy (XPS), binding energy (BE), kinetic energy (KE), linear least squares (LLS), half-width at half maximum (HWHM).

1. Introduction

Hot gibbsite Bayer scales are believed to form either by growth, in which a chemical reaction results in nucleation followed by extended scale growth from solution, or by a settling process in which solids simply settle and then undergo cementation. In this fundamental study of gibbsite scale on mild steel the initial reaction/nucleation that occurred under controlled conditions of laminar flow of a synthetic Bayer liquor was studied by X-ray photoelectron spectroscopy (XPS). Use of XPS enabled characterization of the mild steel surface and also allowed the gibbsite formation to be examined before the scale became visible by traditional electron microscopy and microprobe methods.

2. Experimental

2.1 Laminar flow nucleation cell

All of the gibbsite scale nucleation experiments were conducted under conditions of laminar flow of a synthetic Bayer liquor across SAE/AISI 1020 grade mild steel (typically 0.20% C, 0.50% Mn, 0.05% P, 0.05% S, 0.23% Si) coupons 13 mm in diameter and 2 mm thick. To attain the laminar flow a commercial laminar flow chamber (Vacu-Cell™, C&L Instruments, model number VC-LFR-25-SS-H, Figure 1(a)) was adapted for use. This nominally gave a controlled laminar flow region over an area of 7 x 9 mm with a fluid depth of 250 μm. The area exceeded the XPS spectrometer field of view so that all the XPS data represented only the laminar flow region. Although designed for biological applications under less severe conditions the laminar flow chamber performed well.

In lieu of the glass cover slip or microscope slide normally attached to the chamber a custom PTFE holder for the mild steel disks was fabricated. The entire flow-through cell used for this study is shown in cross-section in Figure 1(b), with the PTFE sample holder encased in a stainless steel jacket and a PID controlled band heater to regulate the temperature of the sample. The latter was monitored by type-T thermocouple pressing against the rear of the sample. Type-T thermocouples also monitored the inlet and outlet liquor temperatures. The cell was designed to receive a single pass of low particulate synthetic Bayer liquor at an elevated temperature. The liquor was filtered twice through 0.45 μm Millpore membrane and stored at room temperature in a liquor reservoir before being pumped via a double head peristaltic pump into a 500 ml stainless steel jacketed vessel

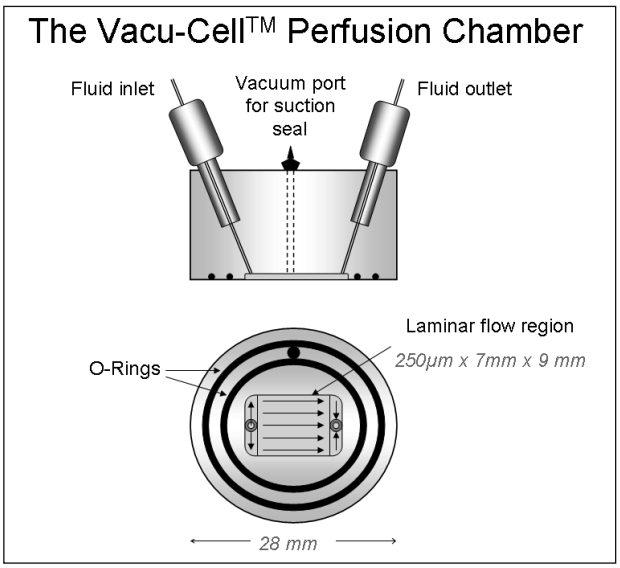

Figure 1(a). Commercial section of laminar flow chamber.

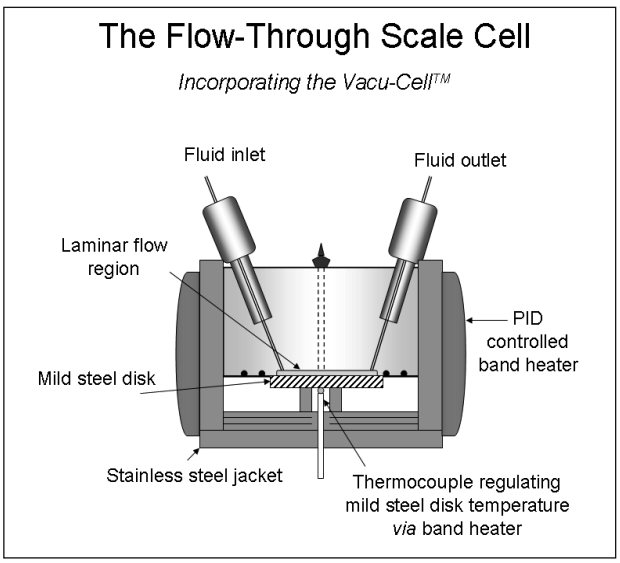

Figure 1(b). Cross-section showing incorporation of a custom sample holder for the mild steel disks.

which acted both as a combined pulse dampener and pre-heat stage for the liquor. One head of the peristaltic pump injected the liquor into the laminar flow cell and the other head acted to remove it. With the double annulus vacuum o-ring seal acting to press the sample and PTFE holder to the laminar flow zone care needed to taken not to over-pressurize the flow chamber.

The Vacu-Cell™ is rated for flow velocities to 0.2 m/sec (presumably because of its normal attachment to thin glass cover slips) but with the custom adaptation was found to work well up to 0.5 m/sec. Because the laminar chamber height is very low at 250 μm, the Reynolds number at the maximum flow used in this work is commensurately low with Re~75, well below a turbulent flow value of 1600.

A total of 13 scale runs are reported in this work. All used a synthetic Bayer liquor with a nominal alumina value A of 150g/L (Al_2O_3) a caustic value C of 220g/L (Na_2CO_3) hence an A/C of 0.7 and a liquor and steel disk temperature of 70°C. The average measured super-saturation in alumina value was 2.3 (Rosenberg and Healy, 1996). Good temperature control over the period of the scaling runs was the most difficult aspect to control. To obtain a disk temperature of 70±2°C (and hence implied liquor temperature) via the PID controlled band heater for the cell the inlet liquor temperature needed to be tweaked depending on the liquor flow rate. At a low flow rate the feed liquor generally needed to be at a higher temperature. Contact times were between 5 and 90 minutes at one of four nominal liquor velocities of 0.06, 0.24, 0.38 and 0.51 m/sec. The experimental matrix reported here consisted of the 4 flow rates each for 30 and 75 minutes contact time and 6 contact times for the medium flow rate of 0.24 m/sec and one replicate. Liquor turbidity and trace Ca level was also monitored (average 2.80 ppm). Surface preparation of the mild steel disks consisted of sequential polishing on SiC wet and dry paper (using Milli-Q water as a lubricant) through the grades of 400, 600, 1200 and finally 2000 grit. This gave a good mirror finish to the surface. From SEM examination the majority of surface scratches were approximately 0.5-1 μm wide. Prior to mounting in the laminar cell the steel disks were de-gaussed (to remove residual magnetism) and sequentially cleaned ultrasonically in a sequence of hexane, acetone and Milli-Q water to endeavour to reduce the adventitious carbon signal typically observable in the XPS. After the scaling runs the surface of the steel disk was further rinsed with Milli-Q water to remove all liquor traces and any subsequent alumina crystallization that might result from entrained liquor evaporation or possibly settled particulates. The sample disk was removed from the PTFE holder and mounted into the XPS stub via a screw attachment.

2.2 Empirical XPS

X-ray photoelectron spectra were obtained using a VG Escalab Mk II (nominal base pressure <1 $x10^{-10}$ mbar) instrument retrofitted with five-channeltron electron detection and an SSI Al K_α monochromatic source in addition to the original Mg K_α and Al K_α twin-anode source. All spectra of the mild steel test disks were acquired with unmonochromated Mg K_α (1253.6 eV) and Al K_α (1486.6 eV) at 300W, irradiated over the whole sample at 50° off-normal. In all cases 6 mm analyser slits (A1) and a constant analyser pass energy (CAE) of 20 eV for narrow region scans and 50 eV for survey scans were used. Each sample was analysed in an identical fashion, acquiring in sequence the combined Al 2s, 2p, Fe 3s, 3p region, O 1s region, Na 1s region, an extended near valence band region from 150 eV and a survey over 1100 eV with Mg K_α radiation followed by the C 1s, O 1s, Fe 2p regions and another 1100 eV survey with Al K_α radiation. The Mg source gives better resolution, but the Al source is required to prevent pronounced Na KLL Auger peak interference with the C 1s and O KLL with the Fe 2p. It should also be noted that the Fe $L_1M_{23}M_{23}$ and L_2VV interferes with the O 1s under Mg K_α radiation. All spectra were acquired with 100 meV channel widths and 100 ms dwell time per channel (50 ms for the survey runs) with number of scans varying from 5 to 50 depending on the region. The specimens were maintained at a temperature of ~150K throughout the XPS to minimize any thermally induced damage and no indications of any radiation damage were evident for any of the spectra. This is more data than is typically acquired in a surface investigation but gibbsite scaling on mild steel presents with the difficulties of a low X-ray photoemission cross section for Al 2p (e.g. for Mg K_α approximately $1/30^{th}$; 0.5735 compared to Fe 2p of 15.97, (Scofield, 1976)), plus the complexities of iron spectra and the Auger overlaps. For most iron-based systems the Fe 2p is the level of choice but the Fe 3p in particular, with its higher KE, enables scale and oxide thickness to be better tracked. By following both the Al 2s and Al 2p changes in concentration, oxidation state and static charging can be double-checked. The extended valence band region is not specifically analysed in this work and will be discussed elsewhere. The C 1s is primarily used as BE calibration check and to monitor carbonate. The survey spectra serve to check for minor Auger peak identification and the possibility of system contamination.

To assist with the correct characterization of the iron oxide surface phase, comparative standards were run on atomically clean 1020 mild steel (cleaned via Ar ion bombardment) and natural mineral samples of hematite (Goose Green mine, Cumbria UK), goethite (Slim Pickens Pocket, Dreamtime Claim, Lake George, Colorado, USA) and magnetite (Mina Huaquio Potosi, Bolivia). The minerals were cleaned and crushed immediately prior to analysis; both the goethite and magnetite were crushed in a nitrogen purged glove-box attached to the XPS spectrometer.

2.3 Predictive XPS

One of the key aspects in using XPS as a quantitative tool is to try and predict expected surface phase compositions, i.e. actual detected intensities, in terms of some surface phase structure. This is particularly important for a study such as scale nucleation. Tabulated surface phase compositions are most often reported on the basis of uniform spatial distribution and no correction for depth dependence. This can be very misleading in terms of the actual surface phase structure. Complex surface phase structures and the expected XPS intensities are difficult to calculate, and in the limit of multiple phases and morphologies, not distinguishable. However simple systems can be predicted and differentiated by combining a good model for photoelectron attenuation such as the TPP-2M model (Tanuma *et al.*, 1994) and estimates for partial photoelectron cross-section such as Scofield, (1976). The TPP-2M model is relatively simple to implement; for a given photoelectron kinetic energy an attenuating phase need only be described in terms of a bulk density, the number of valence electrons per atom, a formula weight and a band gap (if applicable). Scofield gives good partial photoelectron cross-sections for both the Mg K_α and Al K_α X-ray sources so a calculation of expected relative line intensities requires only a numerical integration of photoemission from a source atom density passing through a stipulated phase or set of phases of given dimensions. In practice this numerical integration need only be performed over ~10 nm in depth (typically 45 atomic layers) and is easily achieved within a spreadsheet framework. The result is a calculation of the expected relative photoelectron line intensities for any surface structure model input into the spreadsheet that can then be compared to actual experiment. Note that X-ray depth penetration is large, hence not a factor, and when properly corrected the energy dependence of the transmission function for the Escalab Mk II using the C1 slit (equivalent to the A1 slit for the Escalab 200) actually varies only a few percent over almost 700 eV (Flament and Druet, 1990) which is well within the Fe 2p to Fe 3p region. Morphology is important if the surface phase dramatically differs from the underlying substrate, however where the surface phase morphology follows

the substrate, such as for scale dimensions minor compared to original substrate scratches, the morphology can be ignored. Similarly, for photoemission collected along surface normal (as in this case) angular effects can be ignored.

3. Results

3.1 XPS data analysis strategy

Two data analysis strategies were employed; conventional peak fitting and chemical state assignment (primarily for the Al 2p and O 1s) and linear least squares (LLS) fitting of empirical components for the Fe 2p and Fe 3p. Reliable analysis of Fe 2p spectra is not straightforward. Primarily this is because the multiplet splitting for the ferrous and ferric states broadens the peak structure and makes any peak fit analysis of a mixed oxidation system (Fe^0, Fe^{2+} and Fe^{3+}) subject to major errors; this is particularly the case when trying to characterize a multiple surface phase system with contributions from phases attenuated as a function of depth. When this problem is combined with the inherent errors associated with determining the inelastic photoelectron background the problems are significant, even more so as the various iron oxides can have insulator or semiconductor characteristics and hence display very different relaxation effects. This problem for single phase systems is discussed a number of times in the literature, e.g. Grosvenor *et al.* (2004). Aronniemi *et al.*, (2005, 2007) cover issues of the relative merits of background algorithm and the use of factor analysis on the iron system. Depending on the approach the errors can be substantial. In a more complex real oxide system (electrochemically passivated stainless steel) Yamamura *et al.* (2005) clearly demonstrate that the errors with the peak fitting approach can easily be 50% or more. The LLS approach can be undertaken with or without background correction; as background algorithm choice can increase the quantitative analysis (i.e. the proportion of a given chemical state) error alone by up to 30% (Aronniemi *et al.*, 2005). In this work the LLS was applied without any prior background subtraction. This is perfectly reasonable as (i) the background is intrinsic to the phase generating the photoelectron structure, (ii) the observed spectrum and background will be a linear combination of the components and (iii) the energy width of even the Fe 2p structure is small compared to the energy dependence of the photoemission attenuation.

The LLS fitting used conventional matrix arithmetic to determine a solution, combined with an iterative analysis that independently shifted the energy scale of all possible components for all combinations to obtain the best solution. This is a principal component analysis in which the physically meaningless abstract components are bypassed in favour of known empirical components. Including energy shifting overcame possible errors that might be introduced by an incorrect static charge shift correction. Overall this LLS approach avoided all complicating aspects such as choice of BE values, multiplet splitting and loss peaks and the inelastic scattering background calculation. In the event of some unusual surface phase structure having formed a poor LLS solution would be evident. In this work both the Fe 2p and Fe 3p were analysed by matrix linear least squares (LLS) fitting of empirical standard spectra (clean mild steel, hematite, goethite and magnetite) to the scaling test surfaces. Note that the matrix solution of what fraction of what empirical component to use is determined by a minimization process as the number of energy channels means that the system is massively over-determined. This makes the method particularly effective at discriminating between solutions, e.g. hematite, goethite and magnetite all have Fe 2p envelopes that display only subtle differences yet the LLS enabled easy discrimination.

3.2 Fe 2p and Fe 3p LLS analysis

Fe 2p and Fe 3p LLS analysis was undertaken simultaneously with all possible components (atomically clean 1020 mild steel, magnetite, goethite and hematite) thereby covering the most likely atomic species of Fe^0, Fe^{2+}, Fe^{3+}, O^{2-} and OH^-. This was applied to the raw XPS data of both the polished mild steel surface prior to exposure to the synthetic Bayer liquor and after each scaling experiment. In all cases the LLS fitting rejected both hematite and goethite as being components, i.e. the surface composition could be best explained with contributions from just 2 phases, the underlying mild steel and an oxide layer consisting just of magnetite. Note that whilst the LLS approach immediately yields a fractional contribution of each of the empirical envelopes, this is *not* the same as a percent contribution of that phase to the overall signal. Actual empirical spectra, even when the standards and unknown are acquired with the same instrument, depend upon things such as detector response and surface morphology of which there is no simple *a priori* means of determining. To overcome this limitation two steps must nominally be incorporated; the relative expected intensity of the pure empirical standards needs to be estimated and some background independent measure of the observed empirical spectrum intensity needs to be determined. In practice the numerical estimates for the pure phases cancel out and so only the second step is required. In this work the intensity of the various standard's Fe 2p intensity was based on the product of the Fe $2p_{3/2}$ peak height and the low BE half width at half maximum (HWHM) of that peak. Use of the low BE edge for HWHM avoided the complications (and errors) of peak component fitting to the very complex Fe 2p system. This product gave a signature Fe 2p emission intensity for each of the standards that was then converted to a normalized fractional Fe 2p photoemission from the known envelope fractions. These fractions are different. The normalized photoemission fractions are directly applicable to the numerical estimates from applying the TPP-2M attenuations and Scofield photoemission cross-sections to a given phase model. Rather than the HWHM and peak height product the total Fe 2p integrated intensity could be used, but this is subject to severe errors of integration because of background determination problems. Another background algorithm independent approach is that of Seah and Anthony (1984).

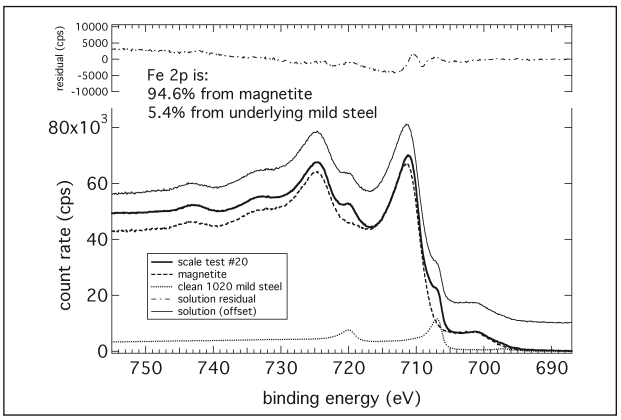

Figure 2. Linear least squares fit of the Fe 2p doublet in terms of underlying mild steel and an oxide layer of magnetite for a typical scaling experiment. Acquired with Al K_α radiation the KE of the photoelectrons involved varies from ~730 to 800 eV.

Figures 2 and 3 show for illustration the resultant LLS fit to the Fe 2p and 3p envelopes for one of the scaling tests (30 minutes at 0.06 m/sec) where the empirical spectral fit percentages of "98.4%" for Fe 2p magnetite and "96.2%" for Fe 3p were converted to actual magnetite values of 94.6% and 88.5% respectively by using the above normalization. What is immediately obvious is that with the higher KE of the photoelectrons in Figure 3 the underlying contribution from the unoxidized mild steel substrate more than doubled from 5.4% to 11.5%. This is a direct illustration of the reduced attenuation at higher kinetic energy. Moreover, it shows quantitatively that any surface phase analysis that simply

reports values of "atomic %" without qualifiers is essentially meaningless. Table 1 shows the LLS results for the Fe 2p and Fe 3p peaks for the full set of scale tests.

Firstly quantification of the Al 2p is complicated by a substantial Fe 3p shake-up feature on the high BE side of the Fe 3p that complicates determination of a conventional background. To

Table 1. The LLS determined steel and magnetite percentage contribution to the Fe spectrum for the 2p doublet and 3p lines and total O 1s to Al 2p ratios for polished disk, blank and subjected to 13 scale tests (one replicate).

		Al K_α		Mg K_α		Mg K_α		
time (min)	flow rate (m/s)	Fe 2p Fe^0	Fe 2p Fe_3O_4	Fe 3p Fe^0	Fe 3p Fe_3O_4	Al 2p (cps.eV)	O 1s : Al 2p	test #
---	---	9.5%	90.5%	18.1%	81.9%	---	---	19
5	0.24	9.1%	90.9%	18.7%	81.3%	4389.5	80.7	12
15	0.24	11.8%	88.2%	22.8%	77.2%	2902.8	125.4	14
30	0.24	8.8%	91.2%	18.1%	81.9%	3165.5	122.9	16
60	0.24	6.7%	93.3%	14.2%	85.8%	2820.4	125.7	15
60	0.24	10.5%	89.5%	20.3%	79.7%	3194.8	122.4	11
75	0.24	6.8%	93.2%	14.7%	85.3%	12508	35.6	18
90	0.24	8.2%	91.8%	16.6%	83.4%	12508	35.5	17
30	0.06	5.4%	94.6%	11.5%	88.5%	2312.8	153.1	20
30	0.38	6.9%	93.1%	15.2%	84.8%	2645.5	124.2	21
30	0.51	9.5%	90.5%	19.3%	80.7%	3312.7	101.0	22
75	0.06	7.2%	92.8%	12.6%	87.4%	10504	36.0	24b
75	0.38	7.3%	92.7%	15.7%	84.3%	4121.7	84.8	25
75	0.51	6.9%	93.1%	16.6%	83.4%	4579.6	75.2	23

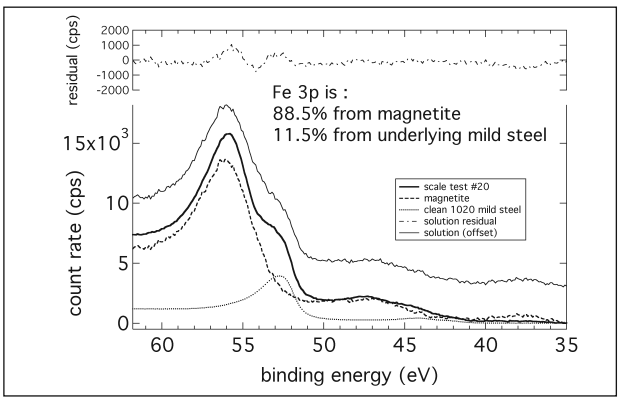

Figure 3. Linear least squares fit of the Fe 3p peak in terms of underlying mild steel and an oxide layer of magnetite for a typical scaling experiment. Acquired with Mg K_α radiation the KE of the photoelectrons involved varies from ~1190 to 1220 eV.

Usually with synthetic component peak fitting the mathematical quality of the fit improves with the number of components used and this causes a dilemma as it encourages false states. By contrast, LLS is particularly sensitive and it will discriminate against false solutions as the fit is determined over a very wide energy range. The percentage contributions in Table 1 should be regarded as an accurate reflection of the mild steel surface post-scaling, the variation (e.g. the replicate) is a consequence of the scaling process. Inspection of Table 1 indicates that little further oxidation occurs after the disks are polished and subjected to the scaling tests.

3.3 Al 2s and Al 2p analysis

Both the Al 2s and Al 2p peaks are relatively narrow and uncomplicated by the photoemission processes affecting the Fe 2p. However, due to a low cross-section the peaks are weak and adjacent to both the Fe 3s and Fe 3p structures. Normally for quantitative work the Al 2p peak is preferred, though slightly weaker than the 2s and nominally a $2p_{1/2}$ $2p_{3/2}$ doublet it is narrower. Both peaks have been followed in this study. Figures 4, 5 and 6 show the Al 2s and Al 2p with a residual Fe 3s for the various scaling tests. This data has been processed in two ways. overcome this all the scaling runs for the Al 2s, 2p and Fe 3s, 3p region had a polished mild steel disk spectrum (no scale and hence no Al signal) normalized and subtracted from the raw data to eliminate this problem. Pre-subtraction was normalized for the Al 2p region so there is some background drift that results for the Al 2s. Also this substantively removed most (but not all) of the underlying Fe 3s. The Fe 3s residual is of particular interest and will be dealt with in a future paper. The second processing step was full width removal of source X-ray line shape and satellite structure by means of a Fourier transform (Klauber, 1993). Without a detailed discussion two points to note are (i) the extended (Gibbs) oscillations on the high BE side of the Al 2s are a boundary artifact of the Fourier transform and relate to the original choice of boundary points for the raw data collection and the regularity of the noise simply reflects the selected frequency cut-off. Note that for all three figures, although the intensity scale has been processed as described, the energy scale is the same as when collected. For comparison the count rate scale is the same in all figures.

Inspection of the spectra reveals a number of characteristics. Firstly the Al 2s behaviour mimics the Al 2p behaviour, both in intensity and shape, the only difference being the better resolution for the Al 2p. Secondly the Al intensity, approximately constant for the varying flow rates at 30 minutes contact time (Figure 4) grows very suddenly after 60 minutes, develops a high BE shoulder which becomes the dominant Al feature (Figure 5) after 90 minutes and that this high BE feature then breaks away and moves even higher in apparent BE (Figure 6).

The initial Al 2p BE is perfectly consistent with Al^{3+} gibbsite ($Al(OH)_3$) and this is essentially invariant across a range of aluminate systems. A slight increase in BE might be expected for Al bound to a highly electronegative anion such as fluoride, but what was observed in the data were two substantial and sudden changes of firstly ~3 eV and then ~9 eV. Both are indicative of static charging processes where the loss of electronic charge via photoemission is not compensated by a flow from earth (due to reduced conductivity) and parts of the surface phase become positively charged and the emitted photoelectrons appear to have a higher BE value. The smaller shift was differential charging

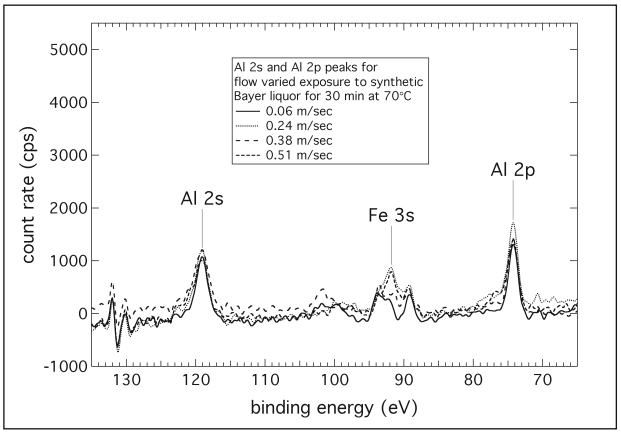

Figure 4. Al 2s and Al 2p region (processed) for mild steel disk exposed to synthetic Bayer liquor at 70°C with varying laminar flow rates for 30 minutes.

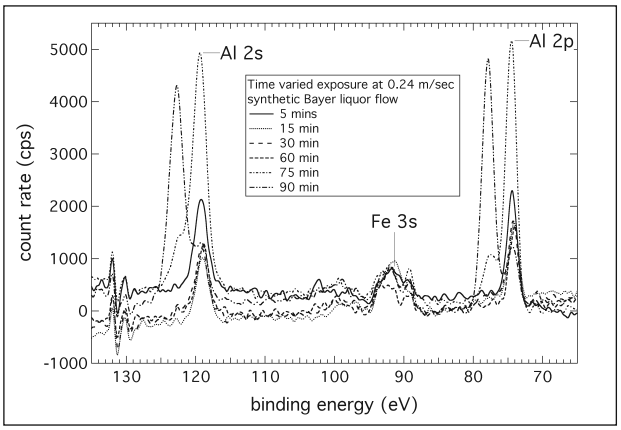

Figure 5. Al 2s and Al 2p region (processed) for mild steel disk exposed to synthetic Bayer liquor at 70°C and a laminar flow rate of 0.24 m/s for varying times.

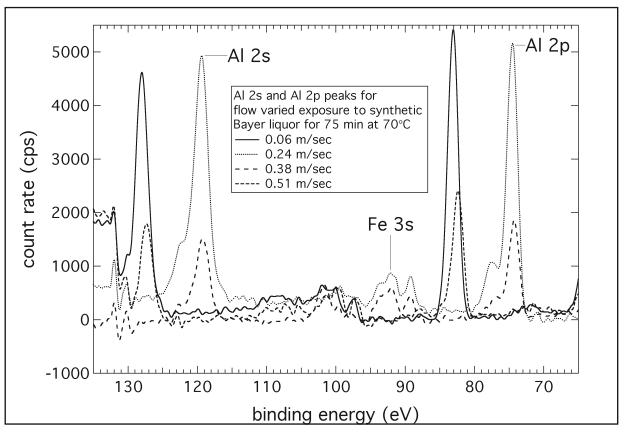

Figure 6. Al 2s and Al 2p region (processed) for mild steel disk exposed to synthetic Bayer liquor at 70°C with varying laminar flow rates for 75 minutes.

that affected part of the Al and O peaks, the larger shift applied to the entire surface and all spectral components. This is an important diagnostic point as it demonstrates the precipitating gibbsite has at least two morphological steps.

4.1 Modelling the Fe 2p and Fe 3p magnetite layer

The primary influence on the attenuation of the bulk Fe^0 signal from the underlying mild steel arose from the initial oxidation causing the formation of a magnetite layer. Using the TPP-2M attenuation estimates and the Scofield cross-sections it is simple to calculate estimates for the magnetite percentage in the Fe 2p and Fe 3p signals. For a magnetite only overlayer model this is shown in Figures 7 and 8. The non-vertical correlation in Figure 8 indicates inadequacy in the model, pointing toward a necessary gibbsite incorporation.

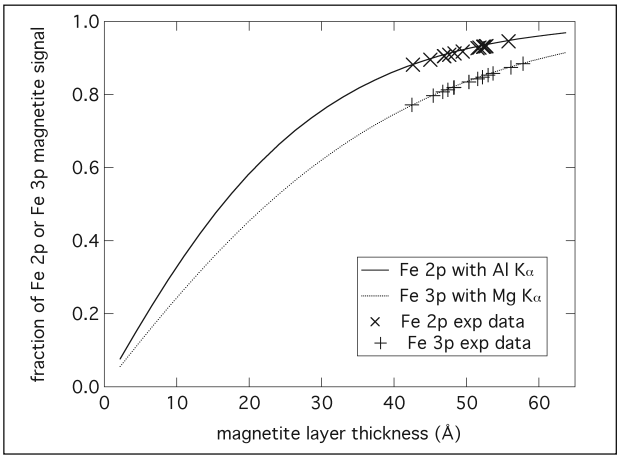

Figure 7. Calculated fractional magnetite signal as a function of magnetite layer thickness with scaling test data overlaid. Empirical magnetite fraction (Table 1) was used to determine a magnetite thickness.

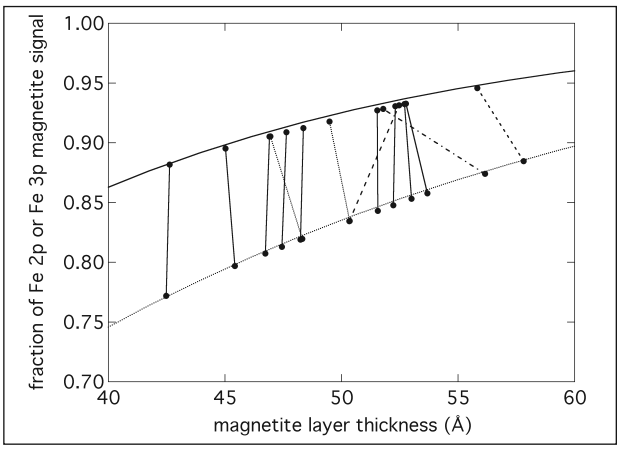

Figure 8. Enlargement of the area of interest in Figure 7 showing the effect of the simple magnetite overlayer model. If the model is correct then the Fe 2p and Fe 3p estimates for each scaling experiment should correlate, i.e. the connected pairs should be vertical.

4.2 Modelling the magnetite layer with gibbsite

As indicated this study reports only on a partial analysis of the scaling experiments undertaken to date and the nucleation model will be refined and reported elsewhere. A preliminary analysis has shown that varying magnetite layer thickness over the range of 19 to 26 layers with varying gibbsite can accommodate the deviations noted in Figure 8; moreover there are multiple indicators to the nucleation process. Just as the Fe 2p and Fe 3p LLS analysis enables a first pass interpretation on the magnetite oxide layer, a simple approach to gibbsite quantification is to analyse the empirical O 1s (total) : Al 2p intensity ratio as a function of the Al 2p intensity. The latter directly gives a gibbsite quantity whilst the ratio ties in the magnetite layer underneath. This initial model did not require a separation of the magnetite oxygen from the gibbsite oxygen.

The data in Table 1 shows a data cluster for the O 1s: Al 2p ratio and absolute Al 2p intensity for those scaling runs at the intermediate flow rate between 15 and 60 minutes that was used to tie in a predicted response to actual measured intensities. These are all thin layer gibbsite with no static charging and most likely represent monolayer or near monolayer gibbsite coverage. Averaging the clustered values gives O 1s: Al 2p of 124.1 and an Al 2p integral of 3020.9 cps.eV. Again, employing the TPP-2M-Scofield numerical integration it is possible to predict the relative XPS intensities for a combined gibbsite-magnetite-steel surface structure. Figure 9 shows the predicted outcome of a gibbsite model with two morphologies with scaling for the Al 2p intensity provided by the above average. Note in particular that only by

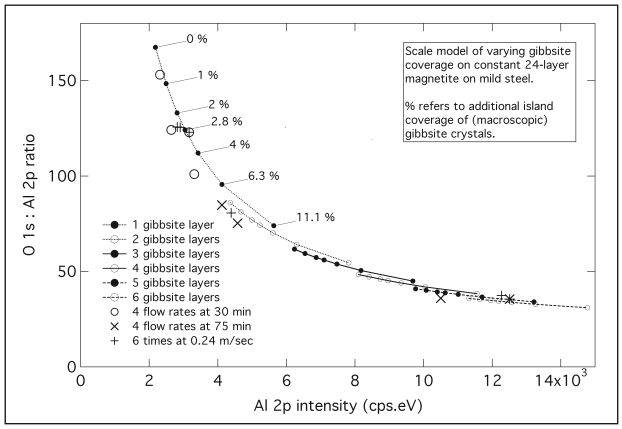

Figure 9. Predicted and experimental O 1s (total) and Al 2p (gibbsite) response for a model based on even gibbsite layers forming on a magnetite-steel surface with additional island coverage of thicker gibbsite crystals.

fixing the empirical data at one point, all points lay very close to the predicted curve.

For the model here the magnetite layer was kept at an even 24 layers (~5.3 nm thick) and then 1 through to 6 even gibbsite monolayers (~0.2 to 1.2 nm) were added. As the gibbsite layer structure becomes thicker the Al 2p intensity continues to increase but the O 1s : Al 2p plateaus as the thicker layers reduce the oxygen contribution from the underlying magnetite. Although not evident from Figure 9 the Al 2p intensity would terminate at ~3x the maximum value shown, i.e. for a sufficiently thick gibbsite layer. The second morphology involves nucleating fully 3-dimensional isolated XPS macroscopic gibbsite crystals on the even gibbsite overlayer. These are shown in a percentage coverage terms as a progression of 0, 1, 2, 2.8, 4, 6.3 and 11.1% for each of the gibbsite overlayer cases. So 0% means no crystals, (just pure overlayer) and 11.3% means that area percentage of the overlayer has additional 3-D crystals. Figure 9 can be seen to be very sensitive to the surface phase structure for 1-2 gibbsite layers, but loses sensitivity when approaching 6 gibbsite layers. "XPS macroscopic" simply means a crystal with a 3rd dimension sufficiently large that all non-gibbsite signal underneath is attenuated to zero. In practice this means >7 nm or so. Although the morphological interpretations are limited they do indicate specific things. For example the cluster used to fix the empirical data is an even monolayer of gibbsite with ~3% crystal coverage. If there were no additional crystal coverage then the values would lie nearer the 0% point. Note that isolated crystals on bare magnetite would generally give a very different response. Below 6.3% coverage the O 1s : Al 2p is >197 and hence off-scale. Above 6.3% the values would come within range on the O:Al curve, e.g. at 9.8% coverage the values can be matched to the cluster average. This model can be dismissed as the cluster average points used above exhibit no static charging, therefore are primarily representative of a thin even overlayer. It would also be expected to exhibit less Fe signal attenuation. These model refinements will be further explored in a follow-up paper and in particular be tied in with SEM observations and a crystal size/coverage analysis. Points such as the average cluster most likely represented the intermediate but "even" gibbsite case of 1.5 overlayers. Indicators for nucleation of the 3-D XPS macroscopic crystals would be more reliably based on the 3 and 9 eV static charge shift points. Certainly the O:Al can explain the static shifted peaks in terms of O:Al and Al values by virtue of a 6-7 gibbsite layer case, but this requires halving the observed magnetite signal and this is just not observed. The more likely scenario is 1-2 layers of gibbsite and then 3-D crystals. What this XPS modelling cannot reveal is the upper size limit of the "XPS macroscopic" 3-D crystals; crystals of 1-2 μm dimensions at 1/10,000th the coverage would appear the same as crystals of 0.01-0.02 μm dimensions.

5. Conclusions

This preliminary gibbsite nucleation study established that for mild steel exposed to synthetic Bayer liquor (70°C, A 150g/L, C 220g/L) under conditions of laminar flow there was an "instantaneous" precipitation of 1-2 layers of gibbsite over a thicker stable magnetite surface layer. That is, the initial appearance of gibbsite was a reaction phenomenon and not a particulate settling process. Under a variety of flow and time conditions nothing significant happened for times of up to 60 minutes. In excess of that time nucleation of larger crystals then became very apparent, clearly identifiable by 2 stages of static charge shifting. It has been demonstrated that significant insight into the structure of the scaling process can be obtained by quantitative prediction of the XPS peak intensities.

References

ARONNIEMI, M., SAINIO, J. & LAHTINEN, J. (2005) Chemical state quantification of iron and chromium oxides using XPS: the effect of the background subtraction method. *Surf. Sci.,* 578, 108-123.

ARONNIEMI, M., SAINIO, J. & LAHTINEN, J. (2007) Aspects of using the factor analysis for XPS data interpretation. *Surf. Sci.,* 601, 479-489.

FLAMENT, O. & DRUET, E. (1990) Calibration of VG ESCALAB MkII spectrometer for XPS quantitative analysis. *J. Electron Spectrosc. Relat. Phenom.,* 53, 141-52.

GROSVENOR, A. P., KOBE, B. A., BIESINGER, M. C. & MCINTYRE, N. S. (2004) Investigation of multiplet splitting of Fe 2p XPS spectra and bonding in iron compounds. *Surf. Interface Anal.,* 36, 1564-1574.

KLAUBER, C. (1993) Refinement of magnesium and aluminum Kα X-ray source functions. *Surf. Interface Anal.,* 20, 703-15.

SCOFIELD, J. H. (1976) Hartree-Slater subshell photoionization cross-sections at 1254 and 1487 eV. *J. Electron Spectrosc. Relat. Phenom.,* 8, 129-37.

ROSENBERG, S.P. & HEALY, S.J. (1996) A thermodynamic model for gibbsite solubility in Bayer liquors. Fourth International Alumina Quality Workshop, Darwin, June 1996.

SEAH, M. P. & ANTHONY, M. T. (1984) Quantitative XPS: The calibration of spectrometer intensity-energy response functions. 1 - The establishment of reference procedures and instrument behavior. *SIA, Surf. Interface Anal.,* 6, 230-41.

TANUMA, S., POWELL, C. J. & PENN, D. R. (1994) Calculations of electron inelastic mean free paths. V. Data for 14 organic compounds over the 50-2000 eV range. *Surf. Interface Anal.,* 21, 165-76.

YAMAMURA, T., OKUYAMA, N., SHIOKAWA, Y., OKU, M., TOMIYASU, H. & SUGIYAMA, W. (2005) Chemical States in Oxide Films on Stainless Steel Treated in Supercritical Water. *J. Electrochem. Soc.,* 152, B540-B546.